Microscopic quantum dynamics study on the noise threshold of fault-tolerant quantum error correction

Y. C. Cheng and R. J. Silbey*
Department of Chemistry and Center for Materials Science and Engineering, Massachusetts Institute of Technology, Cambridge, Massachusetts 02139, USA
(Received 21 December 2004; revised manuscript received 16 March 2005; published 19 July 2005)

Quantum circuits implementing fault-tolerant quantum error correction (QEC) for the three-qubit bit-flip code and five-qubit code are studied. To describe the effect of noise, we apply a model based on a generalized effective Hamiltonian where the system-environment interactions are taken into account by including stochastic fluctuating terms in the system Hamiltonian. This noise model enables us to investigate the effect of noise in quantum circuits under realistic device conditions and avoid strong assumptions such as maximal parallelism and weak storage errors. Noise thresholds of the QEC codes are calculated. In addition, the effects of imprecision in projective measurements, collective bath, fault-tolerant repetition protocols, and level of parallelism in circuit constructions on the threshold values are also studied with emphasis on determining the optimal design for the fault-tolerant QEC circuit. These results provide insights into the fault-tolerant QEC process as well as useful information for designing the optimal fault-tolerant QEC circuit for particular physical implementation of quantum computer.

DOI: 10.1103/PhysRevA.72.012320 PACS number(s): 03.67.Pp, 03.65.Yz

I. INTRODUCTION

Recent developments in the theory of quantum computation have generated significant interest in utilizing quantum mechanics to achieve new computational capability [1]. A quantum computer can outperform its classical counterpart and provide efficient ways to solve many important problems. However, the intrinsic sensitivity of a quantum superposition state to imperfect operations and interactions with its surrounding environment prohibits the realization of a scalable quantum computer. To combat the inevitable errors and decoherence of quantum states during the process of computation, quantum error correction (QEC) and fault-tolerant methods of quantum computation have to be applied in the construction of large-scale quantum computers. It has become clear that the future of robustly storing and manipulating quantum information relies upon the success of fault-tolerant quantum error correction [2–4].

Fault-tolerant methods combined with concatenated coding yield the threshold result, which states if the noise level per elementary operation is below a threshold value, then arbitrarily long quantum computation can be achieved using faulty components [5–9]. Using a t-error-correcting code, fault-tolerant circuits constructed from faulty gates with error rate ϵ can achieve a logical error rate of $O(\epsilon^{t+1})$ per logical gate. This fact together with the concept of concatenated coding provides a method for possible large-scale quantum computation and can lead to the realization of a scalable quantum computer. Therefore, it is important to study fault-tolerant methods and estimate the noise threshold values. In addition, the noise threshold indicates the tolerable noise level in a certain quantum circuit and provides a benchmark for the efficiency of QEC circuits.

A number of theoretical estimates of noise threshold and improvements for the efficiency of QEC circuits have been proposed [5–8,10–12]. In general, these analyses are all based on the following *standard assumptions in QEC*: (1) uncorrelated and stochastic errors, (2) depolarizing noise channel, (3) maximal parallelism, (4) low noise level in storing qubits, (5) no leakage errors, (6) fresh supply of ancilla qubits, and (7) no overhead for performing gates acting on distant pair of qubits. Realistically, these assumptions are not usually applicable, and the power of fault-tolerant QEC under realistic physical conditions is still unclear (see Ref. [8] for a thorough examination on these assumptions). In particular, assumptions (3) and (4) are unlikely to be fulfilled in real physical systems, and these *ad hoc* classical stochastic noise models all neglect device details. We emphasize that noise threshold values are of little use if limitations of the physical implementation and realistic noise sources are not considered in the estimation. Therefore, it is of importance to study fault-tolerant QEC circuits using a noise model that reflects realistic device conditions.

In Ref. [13], we applied a stochastic Liouville equation approach to study the effect of noise in quantum teleportation and controlled-NOT gate operation. Starting from a effective system Hamiltonian that incorporates stochastic fluctuating terms to describe the effect of system-environment interactions, this model can describe the dissipative dynamics of a many-qubit system under realistic device conditions. In this paper, the same approach is applied to investigate the performance of fault-tolerant QEC circuits, implementing three-qubit bit-flip and five-qubit codes. Relatively small codes are studied because we perform a systematic investigation of several variables that can affect the performance of fault-tolerant QEC circuits. In Sec. II we first present the model Hamiltonian we used to implement quantum gates and briefly review the noise model we proposed. The stochastic Liouville equation approach we used allows us to use a more

*Electronic address: silbey@mit.edu

realistic noise model and avoid standard assumptions (2), (3), and (4). We then introduce the fault-tolerant QEC circuits studied in this work in Sec. III and show our estimates of noise threshold in Sec. IV. Finally, we go beyond standard QEC and perform a systematic study on how factors like imperfect measurement, collective bath, repetition protocol, and level of parallelism affect the performance of fault-tolerant QEC in Sec. V. This theoretical study will be useful for the design and implementation of fault-tolerant QEC circuits. We then briefly conclude our results in Sec. VI.

II. INTERACTIONS AND NOISE MODEL

We study the performance of fault-tolerant QEC circuits using a microscopic noise model described in Ref. [13]. In this model, a n-qubit system is described by a Hamiltonian with a controlled part and a time-dependent stochastic part. The general Hamiltonian of the qubit system can be written as ($\hbar=1$)

$$\mathbf{H}(t)=\mathbf{H}_0(t)+\mathbf{h}(t), \tag{1}$$

where the controlled Hamiltonian $\mathbf{H}_0(t)$ describes the interactions between qubits and the stochastic part $\mathbf{h}(t)$ describes the fluctuations of the interactions due to the coupling to the environment. During the process of quantum computation, $\mathbf{H}_0(t)$ is controlled to implement gate operations, whereas $\mathbf{h}(t)$ is stochastic and results in the decoherence of the quantum system.

We choose to simulate fault-tolerant QEC circuits using a model control Hamiltonian with single-qubit X and Z and two-qubit ZZ interactions:

$$\mathbf{H}_0(t)=\sum_{i=1}^{n}\varepsilon_i(t)Z_i+\sum_{i=1}^{n}J_i(t)X_i+\sum_{i=1,j<i}^{n}g_{ij}(t)Z_iZ_j, \tag{2}$$

where Z_i and X_i are Pauli operators acting on the ith qubit and $\varepsilon_i(t)$, $J_i(t)$, and $g_{ij}(t)$ are controllable parameters that can be turned on and off to implement desired gate operations. For simplicity, all gate operations are simulated using step function pulses with field strengths set to 1 (uniform field strengths) and the "on-time" of each pulse is controlled to obtain the desired unitary transformations. Note that by doing so we adopt a dimensionless system in which a unit time scale Δt is defined by the field strength ε—i.e., $\Delta t=1/\varepsilon$. We consider fault-tolerant QEC circuits composed of single-qubit bit-flip (X), phase-flip (Z), Hadamard (H) gates, two-qubit controlled-Z, and controlled-NOT gates, plus measurement of a single qubit in the computational basis. All these operations can be easily implemented using the model Hamiltonian in Eq. (2). Figure 1 shows the gate symbols and corresponding unitary transformations used in our simulations. More complicated transformations such as controlled-Z and controlled-NOT gates can be trivially constructed using these elementary gates; see Fig. 2.

Note that the set of quantum gates we use is not sufficient for universal quantum computation. To address the noise threshold of universal quantum computation, implementations of more complicated quantum gates such as the logical Toffoli gate (controlled-controlled-NOT) or the logical $\pi/8$ gate ($\pi/4$ rotation about the Z axis) have to be considered [4,14]. However, quantum circuits implementing these nontrivial gates are more complicated and do not directly relate to QEC. In addition, analysis on the noise threshold of the fault-tolerant Toffoli gate has shown that with proper arrangement of QEC blocks, the presence of Toffoli gates only causes minor reduction in the threshold value [9]. Therefore, to demonstrate our methodology and the effect of fault-tolerant QEC, we will focus on quantum circuits performing fault-tolerant QEC and calculate the noise threshold for quantum memory and logical X gate in this paper. All the fault-tolerant QEC circuits studied in this paper can be implemented using the set of quantum gates shown in Fig. 1.

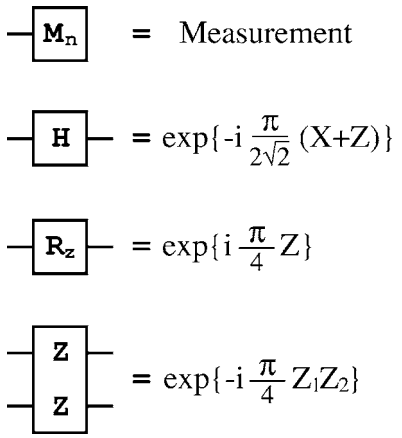

FIG. 1. Quantum gate symbols used to denote unitary transformations implemented with single-qubit X and Z and two-qubit ZZ interactions.

We adopt the ZZ-type two-qubit coupling in our model Hamiltonian for illustrative purposes. The real form of the interqubit interaction depends on the controllable interactions available for each individual physical implementation. Nevertheless, our model can handle other types of interactions as well, and we expect that the model Hamiltonian we use here can reproduce the same general physical behavior as other two-qubit Hamiltonians.

The dissipative dynamics of the system is governed by the stochastic part $\mathbf{h}(t)$. Following Haken and Strobl [15], we consider the fluctuations as random Gaussian Markov processes with zero mean and δ-function correlation times:

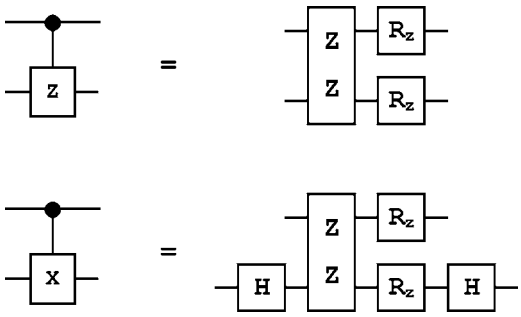

FIG. 2. Constructions used to implement controlled-Z (upper one) and controlled-NOT (bottom one) gates. The definitions of elementary gates are shown in Fig. 1.

$$\langle h_{ij}(t)\rangle = 0,$$

$$\langle h_{ij}(t)h_{kl}(t')\rangle = R_{ij;kl}\delta(t-t'), \tag{3}$$

where the brackets $\langle\cdots\rangle$ mean averaging over the stochastic variables and the time-independent correlation matrix element $R_{ij;kl}$ describes the correlations between $h_{ij}(t)$ and $h_{kl}(t')$. In this paper, we consider the following form of fluctuations:

$$\mathbf{h}(t) = \sum_i \delta\varepsilon_i(t)Z_i + \sum_i \delta J_i(t)X_i, \tag{4}$$

where $\delta\varepsilon_i(t)$ and $\delta J_i(t)$ describe the time-dependent diagonal and off-diagonal fluctuations on the ith qubit, respectively. This corresponds to stochastic single-qubit phase (Z) and bit-flip (X) errors on each individual qubit. In addition, we consider the fluctuations described by the following set of equations:

$$\langle \delta\varepsilon_i(t)\rangle = \langle \delta J_i(t)\rangle = 0,$$

$$\langle \delta\varepsilon_i(t)\,\delta\varepsilon_j(t')\rangle = \gamma_0\delta_{ij}\delta(t-t'),$$

$$\langle \delta J_i(t)\,\delta J_j(t')\rangle = \gamma_1\delta_{ij}\delta(t-t'),$$

$$\langle \delta\varepsilon_i(t)\,\delta J_j(t')\rangle = 0, \tag{5}$$

where γ_0 and γ_1 describe the strength of the diagonal energy fluctuations and off-diagonal matrix element fluctuations, respectively. For a free single-qubit system ($\varepsilon = J = 0$), γ_0 and γ_1 are well-defined physical quantities; i.e., γ_0 and γ_1 are the population relaxation rate and pure dephasing rate, respectively [13]. Note that the noise strengths γ_0 and γ_1 should be interpreted as the error rate per unit time scale $\Delta t = 1/\varepsilon$, where ε is the strength of the control fields. Also notice that we treat the correlation between different qubits independently, which means that each qubit in the system is coupled to a distinct environment (bath). Later we will remove this constraint and examine the effect of a collective bath on the noise threshold value. We also assume that the diagonal and off-diagonal fluctuations are not correlated.

For simplicity, we assume that the noise strengths are uniform; i.e., γ_0 and γ_1 are constants. The noise strength is set to be the same on all qubits at all times; therefore, we do not distinguish storage and gate errors. By assuming that the storage and gate errors are at the same level, the uniform noise assumption overestimates the errors in the system. At the same time it also avoids the weak storage noise assumption usually made in standard QEC. This uniform noise assumption also partly addresses the standard QEC assumption of no overhead for gates acting on distant pair of qubits. Realistically, to perform a quantum gate between two distant qubits in a large-scale quantum circuit, multiple quantum swap gates must be employed to shuffle quantum states around [16]. Our uniform noise assumption reflects the physical condition in this scenario. Note that the assumption of uniform noise strengths is not required in our model; more complex setups, in which control field and noise strengths are different for each individual qubit, can be studied with exactly the same method.

The dynamics of the system is described by the stochastic Liouville equation ($\hbar = 1$)

$$\dot{\rho}(t) = -i[\mathbf{H}(t), \rho(t)],$$

where $\rho(t)$ is the density matrix of the system at time t. Using the method described in Ref. [13] and Eqs. (1)–(5), we can derive the exact equations of motion for the averaged density matrix of the qubit system:

$$\frac{d}{dt}\tilde{\rho}_{\alpha\beta} = -i\sum_j H_{\alpha j}\tilde{\rho}_{j\beta} + i\sum_j \tilde{\rho}_{\alpha j}H_{j\beta} - \frac{1}{2}\sum_{k,l} R_{lk;k\beta}\tilde{\rho}_{\alpha l} - \frac{1}{2}\sum_{k,l} R_{lk;k\alpha}\tilde{\rho}_{l\beta} + \sum_{k,l} R_{\beta l;k\alpha}\tilde{\rho}_{kl}, \tag{6}$$

where all the summations are over all 2^n state indices. In addition, we have defined the averaged density matrix of the system, $\tilde{\rho}(t) = \langle\rho(t)\rangle$. In Eq. (6), the dynamics of the averaged density matrix can be separated into a coherent part, due to $\mathbf{H}_0$, and an incoherent part, due to $R_{ij;kl}$. The dissipation of the system is governed by incoherent dynamics. The time evolution of the qubit system can be obtained by numerically propagating the density matrix of the system using the equations of motion. In our numerical simulation, the density matrix of a system with up to 12 qubits can be easily propagated (bound by the size of physical memory on a personal computer). This method provides an efficient way to simulate quantum circuits and obtain full dynamics of the qubit system.

Although our noise model also assumes uncorrelated and stochastic fluctuations, it is different from classical noise models usually used in standard QEC analyses. The equation of motion (6) treats coherent evolution and incoherent dynamics at the same time and thus includes interference effects between different noise channels and the controlled Hamiltonian $\mathbf{H}_0(t)$. These effects do not exist in classical noise models applied in standard QEC analyses. In addition, our numerical simulation propagates the full density matrix of the system in time; hence the effect of noise is naturally followed by studying the continuous time evolution of the system. Therefore, our method takes into account the state-dependent dissipation and dephasing rates as well as correct propagation of errors in quantum circuits. In standard QEC analyses, state-dependent properties are usually ignored and the propagation of errors is usually included using calculations that require additional approximations [5–8,10–12]. As a result, our noise model not only provides a greater flexibility for including device conditions, but is also a more realistic description than classical noise models.

III. FAULT-TOLERANT QEC CIRCUIT

In this paper, we study fault-tolerant QEC circuits implementing the three-qubit bit-flip code and five-qubit code. We choose to investigate these two codes, because they are relatively small and allow us to perform systematic studies. Previous studies on the fault-tolerant QEC have been mainly focused on Calderbank-Shor-Steane (CSS) codes, especially the CSS [[1,3,7]] code [10,17,18]. Because fault-tolerant en-

coded operations on CSS codes are easy to implement, CSS codes are expected to be more useful for quantum computation than the three-qubit bit-flip code and five-qubit code. Nevertheless, since we focus on variables affecting the performance of fault-tolerant QEC circuits, we expect that results gained in our study can be applied to more general codes. In this section, we introduce these two codes and the methods we apply to perform fault-tolerant QEC.

A. Fault-tolerant QEC scheme

The discovery of quantum error-correcting codes enables us to protect quantum information by encoding [9,17–19]. Although quantum error-correcting codes can correct errors that occur during the storage of qubits, they are unable to protect against errors due to faulty quantum gate operations because multiple-qubit gates can propagate errors and result in uncorrectable erroneous states. A significant achievement in the theory of quantum computation is the discovery of fault-tolerant methods [3]. In the framework of fault-tolerant quantum computation, a quantum error-correcting code is used to encode the quantum information in its logical states (data qubits) and quantum computation is performed directly on the encoded level without decoding. In addition, quantum gates have to be implemented *fault tolerantly*, meaning that a single error happening during a fault-tolerant operation will not lead to more than one error in the outgoing data qubits. Therefore, with high probability errors due to faulty gate operations can be corrected in the subsequent QEC step. By constantly applying fault-tolerant QEC to the data qubits, the accumulation of errors can be decreased. A good introduction to the principle of fault-tolerant QEC can be found in Refs. [8,9].

We adopt the fault-tolerant QEC scheme proposed by DiVincenzo and Shor [3]. This protocol utilizes cat states and transversal controlled-X/Z gates to detect error syndromes and achieve fault tolerance. The fault-tolerant QEC procedure can be divided into three different stages: (1) ancilla preparation and verification, (2) syndrome detection, and (3) recovery.

To detect syndrome fault tolerantly, ancilla qubits have to be prepared in maximally entangled cat states, and go through a verification step to ensure that magnitudes of correlated multiple-qubit errors are small. For example, the four-qubit cat state $(1/\sqrt{2})(|0000\rangle+|1111\rangle)$ is necessary for the fault-tolerant QEC of the five-qubit code. Figure 3 shows the circuit we used to prepare and verify four-qubit cat states [8]. In this circuit, physical qubits are depicted by horizontal solid lines and quantum gates are represented by boxes. An extra qubit is used to detect correlated X errors in the cat state; after the measurement, only states with measurement result equal to zero are accepted. This verification step ensures that a single error in the circuit causes at most a single-qubit error in the final cat state; therefore, the circuit fulfills the fault-tolerant condition. Compared to other fault-tolerant cat-state preparation circuits [1,20], an important feature in the circuit in Fig. 3 is that only a projective measurement is required to verify the cat state fault tolerantly. This is possible because the circuit takes into account the error propagation pattern in the preparation step.

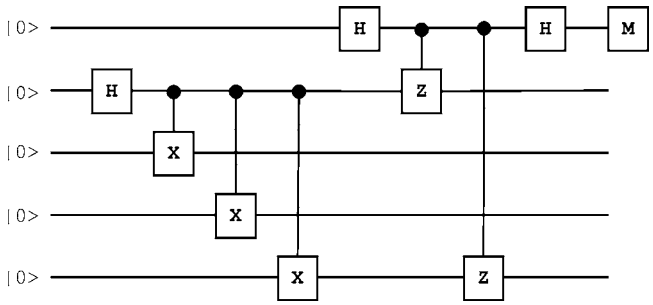

FIG. 3. The fault-tolerant circuit for the preparation and verification of the four-qubit cat state. Note that the final result is conditioned by the outcome of the measurement at the end of the circuit. If the measurement outcome is zero, we accept the state; otherwise, the state is discarded and the circuit is started over again.

To ensure fault tolerance, the ancilla cat state is used to perform transversal controlled-X/Z operations to transfer information about the errors from the data qubits to the ancilla qubits. After decoding the ancilla state, a projective measurement is then applied to obtain error syndromes. Because there are more gates in the circuits than the number of measurements, it is reasonable to assume that the measurement has a smaller effect on the threshold result. Therefore, we assume a perfect measurement. Later we will study the effect of measurement errors. In addition, to ensure that we do not accept a wrong syndrome and mistakenly apply bit-flip or phase-flip gates on the data qubits, we must repeat syndrome detection and take a majority vote. Following Shor's protocol [3], the following repetition scheme is used.

Repetition protocol A (three majority vote):

(i) Perform the syndrome detection twice. If the same measurement results are obtained, the syndrome is accepted and data qubits are corrected.

(ii) Otherwise, perform one more syndrome detection. If any two of the three measurement results are the same, the syndrome is accepted and data qubits are corrected.

(iii) If all three measurement results are different, no further action is taken.

This protocol is basically a simple majority vote in three trials. Note that the choice of the repetition protocol is not unique. In fact, later we will compare protocol A to another protocol, and show that we can improve this protocol to increase the efficiency of the fault-tolerant QEC procedure.

After a syndrome is detected and confirmed, a final recovery operation is carried out to correct the detected error in the data qubit. This completes a fault-tolerant QEC circle.

Combining all these elements, we can ensure that a single error during the fault-tolerant procedure only leads to a single-qubit error in the outgoing data qubits. As a result, all multiple-qubit errors in the outgoing data qubits must be due to multiple error events during the QEC procedure. For example, if the fault-tolerant circuit is constructed from faulty gates with error probability ϵ, the probability of generating a two-qubit error in the data qubit is of order ϵ^2. In fault-tolerant quantum computation, we constantly perform the fault-tolerant QEC on the data qubits. As a consequence, single-qubit errors in earlier computation and QEC steps will be corrected in later QEC steps with high probability (sup-

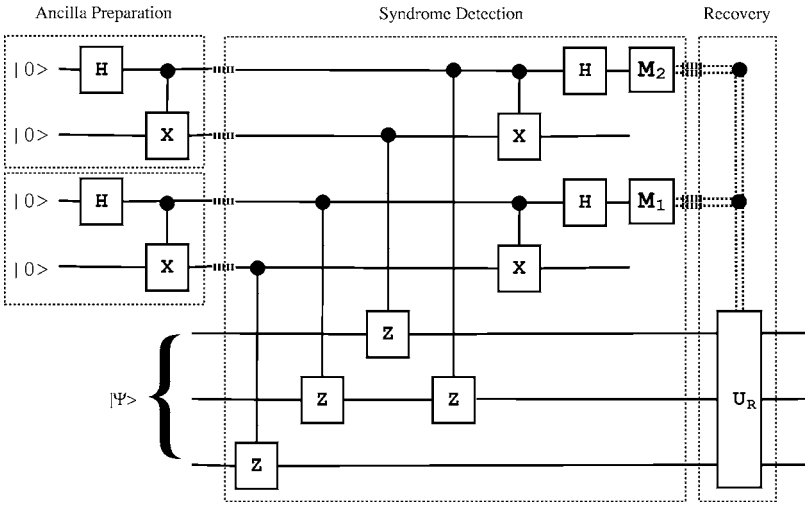

FIG. 4. The fault-tolerant circuit for a QEC step on the three-qubit bit-flip code. Note that to ensure the fault-tolerant condition, the syndrome detection has to be repeated for several times and then the result of a majority vote taken.

pose a single-error correcting code is used). Therefore, single-qubit errors would not accumulate during the process of computation; only multiple-qubit errors will accumulate at a rate of $O(\epsilon^2)$. As a result, we can achieve longer computation when ϵ is small.

B. Three-qubit bit-flip code

The three-qubit bit-flip code encodes a logical qubit in three physical qubits using the following logical states:

$$|0_L\rangle = |000\rangle,$$

$$|1_L\rangle = |111\rangle.$$

The three-qubit bit-flip code corrects the single bit-flip error on any of the three data qubits. This code does not correct phase errors; therefore, it is only useful when the degradation of the quantum state is dominated by bit-flip errors. However, we believe insights gained by studying this code can be applied to more general quantum error-correcting codes.

Figure 4 shows the fault-tolerant QEC circuit for the three-qubit bit-flip code. The quantum circuit includes three data qubits that take a encoded state as the input and two pairs of ancilla qubits that will be prepared in the Bell state $(1/\sqrt{2})(|00\rangle+|11\rangle)$ and used to measure the syndromes. Note that the Bell state is invariant under correlated bit-flip errors (i.e., XX); therefore, no verification step is needed. Figure 5 shows the syndrome detection circuit in detail. We want to point out that only limited ability to perform operations in parallel is assumed in constructing this circuit. In addition, by arranging a two-qubit ZZ gate in front of a single-qubit R_z gate, the circuit minimizes error propagation from the ancilla qubits to the data qubits. At the end of the circuit, two measurements M_1 and M_2 are performed to obtain the error syndrome. After the syndrome is confirmed according to the repetition protocol A, we then apply the corresponding recovery action to correct the detected error. Table I lists the syndrome and the corresponding recovery actions for the three-qubit bit-flip code.

Because the three-qubit bit-flip code only corrects bit-flip errors, we only consider off-diagonal fluctuations on each qubit when dealing with this code ($\gamma_0=0$). Note that the circuit does not protect against Z errors; nor can it prevent the generation of Z errors. To access its performance on controlling X errors on the data qubits, we study the fault-tolerant QEC procedure only when the data qubits are initially in the logical $|0_L\rangle$ state. In our model, using the logical $|1_L\rangle$ state as the initial state will give the same result. This selection of initial state is unrealistic, but it allows us to avoid uncorrectable Z errors that will ruin the QEC procedure.

C. Five-qubit code

The five-qubit code is the smallest quantum code that corrects all single-qubit errors [21,22]. A scheme for fault-

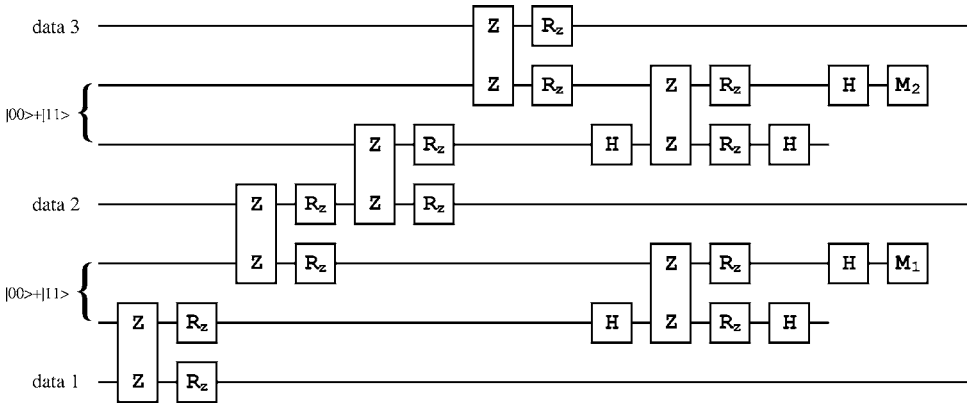

FIG. 5. A circuit implementing the fault-tolerant syndrome detection for the three-qubit bit-flip code.

TABLE I. Measurement results and the corresponding actions required to correct the error in the data qubit for the three-qubit bit-flip code.

Syndrome		Action
M_1	M_2	U_R
0	0	III
0	1	IIX
1	0	XII
1	1	IXI

tolerant quantum computation using five-qubit code is presented by Gottesman in Ref. [4]. Here we adopt the representation and fault-tolerant QEC circuit presented by DiVincenzo and Shor in Ref. [3]. Their implementation uses a nine-qubit system with five data qubits and four ancilla qubits, which utilizes four-qubit cat state $(1/\sqrt{2})(|0000\rangle + |1111\rangle)$ for syndrome detection. Moreover, four syndromes are detected sequentially. It is straightforward to simulate the syndrome detection circuit presented in their paper using our choice of model Hamiltonian [Eqs. (1)–(5)].

Ideally, multiple input states have to be studied to obtain averaged performance of the QEC procedure. To avoid such tedious computations, we use a logical qubit initially in the following pure-state density matrix (in the $\{|0_L\rangle, |1_L\rangle\}$ basis):

$$\rho_0 = \frac{1}{2}\left(I + \frac{1}{\sqrt{3}}X + \frac{1}{\sqrt{3}}Y + \frac{1}{\sqrt{3}}Z\right).$$

This state provides an averaged measure for all possible logical states and thus should give us a reasonable estimate of the averaged circuit performance.

The quantum circuit implementing the decoding, error correction, and decoding of the five-qubit code has been studied experimentally using a NMR quantum computer with five qubits [23]. Note that our setup simulates a minimal circuit for the fault-tolerant QEC using a five-qubit code with limited physical resources. We expect such a nine-qubit system can be realized on a liquid-state NMR quantum computer using available technologies. An experimental study of such a minimal fault-tolerant QEC circuit will be an excellent test for our noise model and can also provide us invaluable information that is essential for the design of large-scale quantum computers.

IV. ESTIMATE OF NOISE THRESHOLD

To estimate the noise threshold for a logical operation, we simulate a computation in which fault-tolerant QEC is performed after each logical operation on the encoded qubits and compare the magnitude of logical errors to the magnitude of errors generated by the same operation on a bare physical qubit without QEC. We use the crash probability P_c to describe the amount of logical errors in an encoded state [11]. The crash probability is defined as the probability of having an uncorrectable error in the data qubits and can be obtained from the fidelity of the state *after a perfect QEC process*. For the single-error-correcting codes used in this paper, the crash probability P_c equals to the probability of having more than one error in the data qubits.

We define a computational step as a logical gate followed by a fault-tolerant QEC step. If the same computational step is applied repeatedly on the data qubits n times, we can describe the crash probability as a function of n—i.e., $P_c = P_c(n)$. In general, $P_c(n)$ satisfies an exponential form

$$P_c(n) = \frac{1}{2}(1 - e^{-2\Gamma_n n}). \tag{7}$$

We can perform simulation and compute crash probability at each step, $P_c(n)$. By fitting our simulation result to the functional form in Eq. (7), we obtain the crash rate constant per computational step $\Gamma_n = dP_c(n)/dn|_{n=0}$. In addition, we also define the crash rate constant per unit time $\Gamma_t = dP_c(t)/dt|_{t=0} = \Gamma_n/\tau$, where τ is the time period required to complete a computational step. Note again that the unit time scale Δt is defined by the strength of control fields ε, $\Delta t = 1/\varepsilon$.

We compute the noise threshold for a quantum memory, where repeated fault-tolerant QEC is applied on the data qubits to stabilize quantum information, and logical X gate, where a logical X gate followed by a fault-tolerant QEC step are applied on the data qubits. Figure 6 shows the crash rate constants as a function of noise strength for the three-qubit bit-flip code, as well as the results for the five-qubit code. In Fig. 6, we clearly see that in the weak noise regime, the crash rate constant is proportional to the square of the noise strength. This is the standard result of fault-tolerant QEC using single-error-correcting codes and reflects the power of the fault-tolerant QEC procedures. The noise threshold can be obtained from the critical value at which the crash rate constant for encoded computation crosses over with the error rate of a bare physical qubit. At noise strength below the threshold value, the errors in the encoded state accumulated slower than for the bare physical qubit. At noise strength above the threshold value, the fault-tolerant QEC provides no benefit. For the three-qubit bit-flip code, the noise threshold is about 2×10^{-2} for quantum memory, and about 1×10^{-3} for the logical X gate.

We also perform calculations on the five-qubit code. Table II summarizes threshold values for the three-qubit bit-flip code and five-qubit code. The five-qubit code corrects all single-qubit errors, so we can compute the threshold for different types of noise. Clearly, there exist minor differences between noise thresholds for different types of noise. In addition, the noise threshold of a quantum memory is about an order of magnitude higher than the threshold of a logical X gate. A closer look indicates that the difference is mainly due to the different bases of comparison. For the quantum memory, we must compare the crash rate constant per unit time Γ_t to the decay rate of a free physical qubit; however, for the X gate, we need to use the crash rate constant per computational step Γ_n. The extra logical X operation has little effect on the crash rate per computational step because the fault-tolerant QEC circuit is much larger than the circuit for the logical X gate. This observation suggests that other

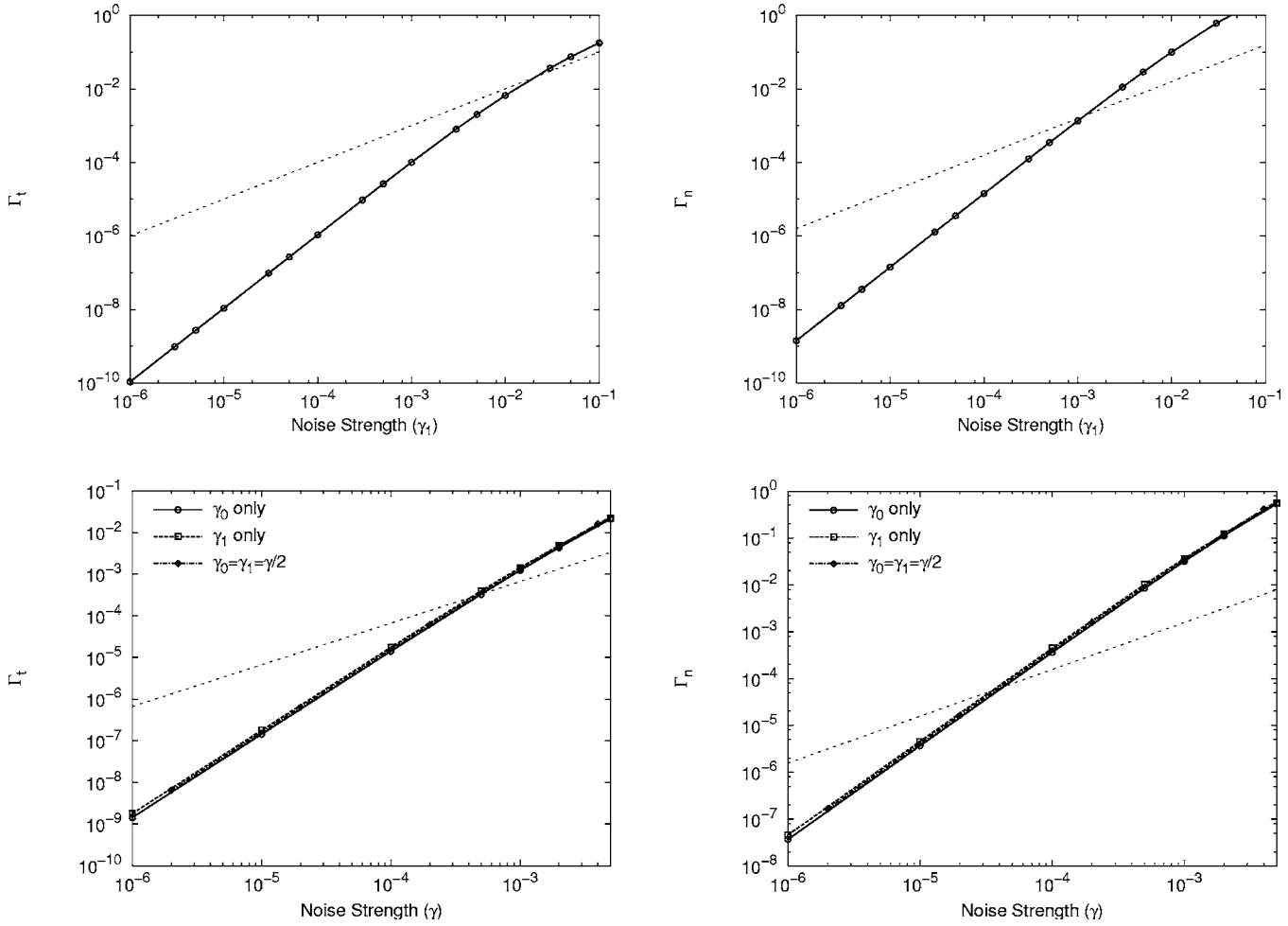

FIG. 6. Crash rate constants as a function of the noise strength. We show crash rate constants for a quantum memory using the three-qubit bit-flip code (upper left) and five-qubit code (upper right) and for a logical X gate on the three-qubit bit-flip code (bottom left) and on the five-qubit code (bottom right). For the five-qubit code circuits, curves for different types of noise are presented. To show the threshold result, we also present curves for the error rate of a single physical qubit (dotted line). The noise threshold values are summarized in Table II.

encoded single-qubit operations and transversal encoded two-qubit operations should have similar threshold values.

For the five-qubit code, our estimate of the noise threshold is about 4×10^{-5} for the logical X gate. Previous threshold calculations have all adopted CSS codes. For comparison, we have followed Gottesman's analysis in Ref. [9] and calculated thresholds of the three-qubit bit-flip code and five-qubit code. Following Gottesman's model, we estimated for the five-qubit code a threshold of 10^{-3} when storage errors are negligible and 2×10^{-4} when the strength of storage errors are equal to gate errors. These values cannot be compared directly to our threshold estimates because the definitions of unit time and error rates are different. Nevertheless, we can draw useful observations from the comparison. Clearly, the limited parallelism in the circuits and the uniform noise assumption that treats gate errors and storage er-

TABLE II. Summary of noise threshold values. The noise strengths (γ_0 and γ_1) should be interpreted as the error rate per unit time scale, $\Delta t=1/\varepsilon$, where ε is the strength of the control fields. For comparison, thresholds obtained from a classical noise model are listed in the parentheses. These numbers are obtained by following Gottesman's analysis in Ref. 9, and all standard assumptions mentioned in Sec. I are applied.

	Three-qubit bit-flip code		Five-qubit code	
	Memory	X gate	Memory	X gate
X errors (γ_1)	2.1×10^{-2}	1.2×10^{-3} (5.8×10^{-3})	4.2×10^{-4}	3.5×10^{-5}
Z errors (γ_0)	—	—	5.1×10^{-4}	4.3×10^{-5}
Both X and Z errors	—	—	4.7×10^{-4}	3.9×10^{-5} (1×10^{-3})

rors on the same footing are responsible for the significantly lower threshold we have obtained for the five-qubit code. Previous calculations have indicated that including storage errors would decrease the threshold value by almost an order of magnitude. Our result implies that without maximal parallelism, there is an order of magnitude reduction of the threshold.

We summarize the assumptions we made for these calculations: (1) stochastic and uncorrelated X and Z noises, (2) each qubit coupled to a distinct bath, (3) uniform noise strength, (4) perfect physical $|0\rangle$ states as initial states, (5) no leakage errors, (6) no overhead for performing gates acting on distant pair of qubits, and (7) perfect instantaneous projective measurement. Compared to the standard assumptions in QEC, we do not assume maximal parallelism and weak storage errors. In addition, our calculations include real construction of quantum gates. Note that up to this point we have basically reproduced the standard results of fault-tolerant QEC using a more realistic noise model. In the next section we will study factors that are usually overlooked in standard QEC analyses and examine how these factors affect the performance of fault-tolerant QEC.

V. EFFICIENCY OF FAULT-TOLERANT QEC CIRCUITS

In this section, we study several variables that can affect the efficiency of the fault-tolerant QEC scheme. The effects of these variables are usually overlooked in standard noise threshold analyses. We perform a systematic investigation on the performance of quantum memories stabilized by fault-tolerant QEC and aim to generate a generic picture on how these variables quantitatively change the efficiency of fault-tolerant QEC circuits. Because our noise model can provide a quantitative description of the efficiency of fault-tolerant QEC circuits including realistic device conditions, the method applied here can be used to benchmark different quantum circuits and search for optimal circuit design for real physical implementations.

A. Effect of imperfect measurement

Previous studies on the noise threshold of fault-tolerant QEC typically treat the measurements as simple one qubit operations [5,7,8,10]. Recently, Steane has studied the effect of measurement time and found that a long measurement time can significantly reduce the noise threshold [11]. Here we test another type of errors due to measurement: namely, projecting to an incorrect state due to imperfect measurement. We assume that the measurement is instantaneous and use the following POVM (positive operator-valued measure) to describe an imperfect projective measurement on a single qubit:

$$M_0 = (1-\eta)|0\rangle\langle 0| + \eta|1\rangle\langle 1|,$$

$$M_1 = (1-\eta)|1\rangle\langle 1| + \eta|0\rangle\langle 0|,$$

where M_0 (M_1) describes events in which the basis state $|0\rangle$ ($|1\rangle$) is measured and η is the probability of measurement error—i.e., a projection onto the wrong basis state. Figure 7 shows curves for the crash rate constant per unit time Γ_t at different probabilities of measurement errors for a quantum memory implementing the three-qubit bit-flip code. Clearly, Γ_t is insensitive to the measurement errors even when the probability of measurement errors is significantly higher than the noise strength γ_1. The probability of the measurement error as high as 5% has only minor effect on the threshold value. This result suggests that a short and less accurate measurement is preferable to a long one.

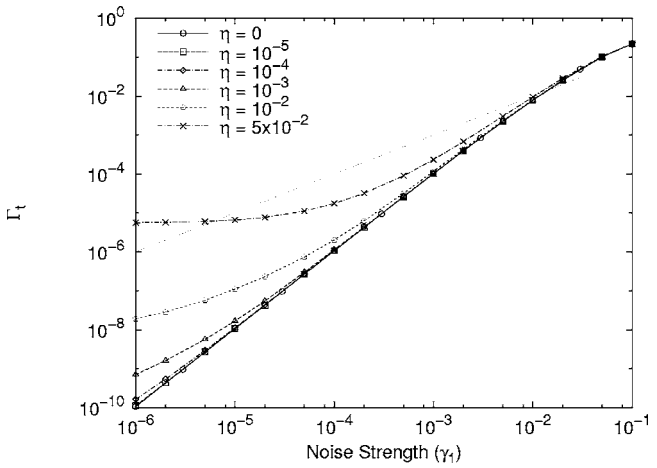

FIG. 7. Γ_t as a function of noise strength for the fault-tolerant QEC circuit using three-qubit bit-flip code at different level of measurement errors. The error rate of a single physical qubit is also shown (dotted line). The measurement error has little effect on the threshold value.

B. Effect of a collective bath

A distinct feature of our noise model is the ability to describe the effect of a collective bath, in which all qubits are coupled to the same environment. Such an environment is relevant in physical implementations such as trapped-ion quantum computers, where qubits are coupled to the same collective phonon modes [24,25]. The effect of a collective bath on the fault-tolerant QEC is an interesting topic. Because a collective bath seems to contradict the idea of uncorrelated and stochastic errors that is the foundation of fault-tolerant QEC, several authors have suggested that collective decoherence has to be avoided for fault-tolerant quantum computing [8,26]. Also, in a collective bath the effects of noise on different qubits add coherently; as a result, super-decoherence states exist and might affect the efficiency of fault-tolerant QEC [27].

To address this question, we simulate the fault-tolerant QEC circuit for the three-qubit bit-flip code using a noise model in which all qubits are coupled to a common bath. The following forms of correlation functions for the stochastic process are used:

$$\langle \delta\varepsilon_i(t)\rangle = \langle \delta J_i(t)\rangle = 0,$$

$$\langle \delta\varepsilon_i(t)\,\delta\varepsilon_j(t')\rangle = \gamma_0\delta(t-t'),$$

$$\langle \delta J_i(t)\,\delta J_j(t')\rangle = \gamma_1\delta(t-t'),$$

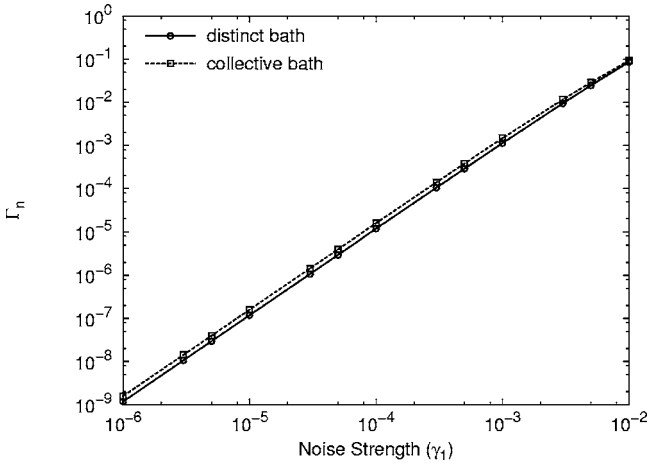

FIG. 8. The crash rate per computational step, Γ_n, for the three-qubit bit-flip code as a function of the noise strength. Curves for the distinct bath system (solid line) and collective bath system (dotted line) are shown. The result for the collective bath is close to the result for localized baths. This result suggests that collective bath has minor effect on the efficiency of fault-tolerant QEC.

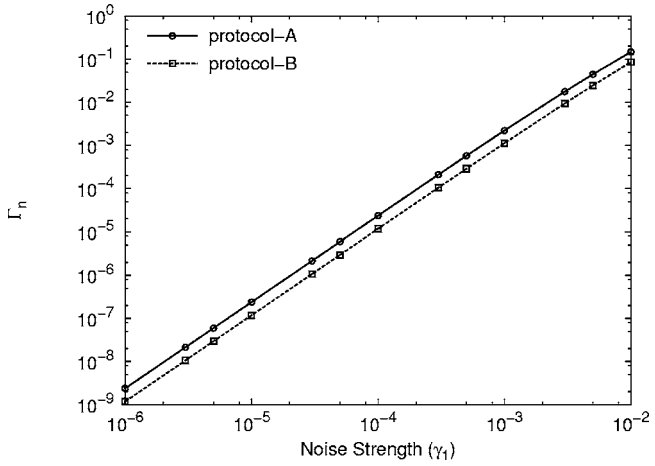

FIG. 9. The crash rate constant per step, Γ_n, as a function of the noise strength for the two different repetition protocols for a quantum memory using three-qubit bit-flip code. Using protocol B reduces the crash rate constant by a factor of 2.

$$\langle \delta\varepsilon_i(t)\,\delta J_j(t')\rangle = 0, \tag{8}$$

Notice that in Eq. (8), fluctuations on different qubits are fully correlated; this reflects the result of coupling to a common bath. Figure 8 shows the crash rate constant Γ_n for quantum memories using the three-qubit bit-flip code with two different types of baths. The crash rate curve for the collective bath case is only slightly higher than the curve for the localized bath, and there is no significant difference between these two lines. This result suggests that a collective Markovian bath, which exhibits spatial but not temporal correlation, has little effect on the efficiency of fault-tolerant QEC. Although superdecoherence states do exist when the system is coupled to a collective bath, they have little effect on the dynamics of the system, because those states represent only a small fraction in the whole Hilbert space. The fault-tolerant QEC circuit using the five-qubit code was also studied, and similar results were obtained.

Fault-tolerant QEC methods might not be the best way to deal with collective decoherence in quantum computation. In a collective bath setup, there exist states that are robust against collective decoherence. These states form a subspace called decoherence-free subspace (DFS) [28,29]. The existence of DFS's has been verified experimentally [30–33]. In addition, by encoding quantum information in the DFS's and performing quantum gates that are strictly inside the DFS's, universal fault-tolerant quantum computation can be achieved without the extensive space and time overheads required for QEC [34–36]. Other proposals that utilize the properties of a collective bath include concatenation of DFS and quantum error-correcting codes [37] and supercoherent qubits [38]. These passive error-preventing schemes are preferable for fault-tolerant quantum computation in collectively decoherent environments. Although our focus in this paper is on QEC methods, it is worth noting that our stochastic Liouville equation approach can be used to study these collective decoherence models. In fact, in Ref. [13] we have theoretically demonstrated a decoherence-free state in a two-qubit system using the same approach. Moreover, in a realistic physical device such as solid-state qubits, the correlation between noise on different qubits is likely to be a function of the distance between the qubits. For example, the correlations of the diagonal fluctuations might exponentially decay in space:

$$\langle \delta\varepsilon_i(t)\,\delta\varepsilon_j(t')\rangle = \gamma_0 e^{-|i-j|/L}\delta(t-t'),$$

where L is a characteristic coherence length of the system. Our stochastic Liouville equation approach can easily model such partially collective baths, and it will be interesting to apply our approach to study DFS methods in these realistic bath conditions.

C. Repetition protocol

Our simulation propagates the density matrix of the system in the process of computation; therefore, we obtain the full information about the time evolution of the system. The ability to obtain the full trajectory of the qubit system is another important advantage of our simulation method. By examining the trajectory of the system during the fault-tolerant QEC process, we find the following repetition protocol yields the best performance.

Repetition protocol B (conditional generation):

(i) Perform the syndrome detection once. If this syndrome is zero, do nothing.

(ii) Otherwise, perform the syndrome detection again. If the same syndrome is obtained, accept the syndrome and correct data qubits accordingly.

(iii) Otherwise, no further action is taken.

Figure 9 shows the crash rate constant Γ_n for quantum memories implementing the three-qubit bit-flip code using different repetition protocols. Because the majority of the measured syndromes will be zero in the weak-noise regime, protocol B reduces the amount of time required for a fault-

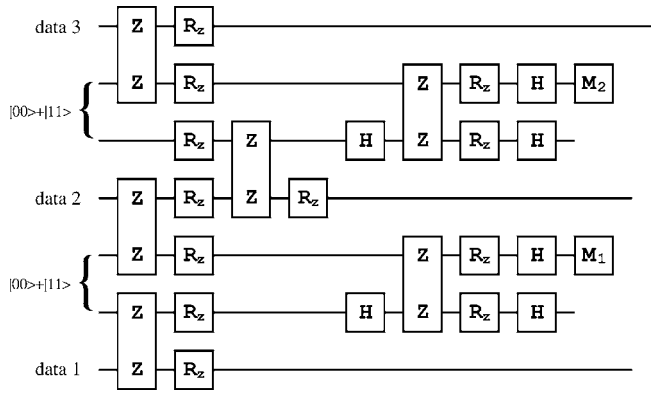

FIG. 10. A circuit implementing the fault-tolerant syndrome detection for the three-qubit bit-flipping code. In this circuit, we assume that the quantum computer can perform quantum gates on different qubits in parallel.

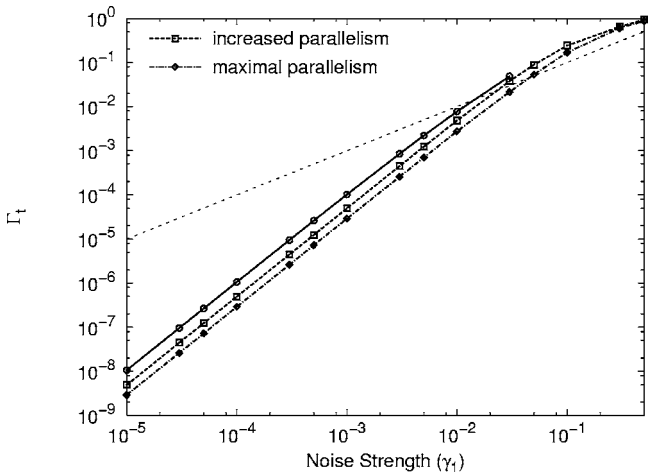

FIG. 11. The crash rate constant per unit time, Γ_t, as a function of the noise strength for quantum memories using the three-qubit bit-flip code. Curves for three syndrome detection circuits different in the level of parallelism are shown. The solid line is for the circuit shown in Fig. 5, the dashed line is the increased parallelism circuit shown in Fig. 10, and the dash-dotted line is the maximal parallelism circuit that finishes all controlled-Z operations in a single pulse. We see dramatic improvement in the noise threshold values when the level of parallelism is increased. The result indicates that by increasing the level of parallelism, the threshold value can be significantly improved.

tolerant QEC step by a factor of 2. As a result, the crash rate constant per computational step, Γ_n, decreases by a factor of 2 when protocol B is used. Similar improvements on the fault-tolerant QEC protocol have been suggested by other groups [11,12,39]. The idea behind protocol B is that the syndrome detection circuit is complicated and generates extra errors on the data qubits, therefore minimizing the number of syndrome detection and accepting a syndrome only when two consecutive detections agree on the same syndrome improve the efficiency of the fault-tolerant QEC procedure.

D. Level of parallelism

An important factor related to the efficiency of a QEC circuit is the level of parallelism in the circuit. The level of parallelism available is determined by the computing device, but previous threshold calculations typically ignore this issue. The syndrome detection circuit shown in Fig. 5 assumes a restricted level of parallelism. In fact, for a reasonable physical implementation, gate operations on different qubits might actually be operated in parallel to reduce the operation time. For example, a quantum computer implementing Kane architecture is capable of performing controlled-Z gates in parallel on different pairs of qubits [40]. Figure 10 shows a compressed version of the syndrome detection circuit that has increased level of parallelism.

Furthermore, because the interactions used to implement the controlled-Z gate commute with each other (Z_i and Z_1Z_2 commute), in principle the controlled-Z gate can be made in one step:

$$\text{controlled-}Z = e^{-i\pi Z_1 Z_2/4} e^{i\pi(Z_1+Z_2)/4} = e^{-i\pi(Z_1Z_2-Z_1-Z_2)/4}.$$

This makes it possible to perform a controlled-Z operation in a single pulse. This maximal parallelism design is a theoretical model used to benchmark the maximal gain available from the increase of parallelism. This design does not correspond to any physical implementation, and is a special case for our choice of model interactions (ZZ coupling).

Figure 11 shows the crash rate constant per unit time Γ_t for quantum memories implementing the three-qubit bit-flip code. Results for three syndrome detection circuits with different levels of parallelism are shown. The noise thresholds for the original circuit (Fig. 5), increased parallelism circuit (10), and maximal parallelism circuit are approximately 1.5×10^{-2}, 2.3×10^{-2}, and 4.6×10^{-2}, respectively. The results indicate that by increasing the level of parallelism, the noise threshold can be significantly improved. Note that the reduction of the operation time in higher level of parallelism cannot account for all of the improvement on the threshold values; because the crash rate constant per unit time Γ_t has been scaled by the amount of time needed to complete a fault-tolerant QEC step ($\Gamma_t=\Gamma_n/\tau$), any difference in Γ_t is from sources other than difference in τ. The improvement in the threshold value is because when the level of parallelism is increased, the number of pathways that generate uncorrectable errors decreases. Finally, we emphasize that our method can access the real threshold value, reflecting the limitations of an individual computing device.

VI. CONCLUSION

We have applied a noise model based on a generalized effective Hamiltonian to study the effect of noise on the performance of fault-tolerant QEC circuits. The model includes realistic physical interactions for the implementations of quantum gates and describes the effect of system-bath interactions by including stochastic fluctuating terms in the system Hamiltonian. As a result, this method simulates quantum circuits under physical device conditions and gives us a full description of the dissipative dynamics of the quantum computer.

Fault-tolerant QEC circuits implementing either the three-qubit bit-flip code or the five-qubit code were investigated, and the noise threshold for quantum memory and logical X gate were calculated by comparing the logical crash rate to the error rate of a bare physical qubit. The noise threshold of quantum memories using the three-qubit bit-flip code and five-qubit code is about 2×10^{-2} and 5×10^{-4}, respectively. The noise threshold of logical X gates using the three-qubit bit-flip code and five-qubit code is about 1×10^{-3} and 4×10^{-5}, respectively. Note that in our dimensionless system, these noise strength values should be interpreted as the error rate per unit time scale, $\Delta t=1/\varepsilon$, where ε is the strength of the control fields. These threshold values are obtained from a uniform noise model where the magnitudes of storage errors and gate errors are the same. This result indicates that fault-tolerant quantum computing is possible in systems with strong storage errors. A possible scenario for such a system is the linear nearest-neighbor architecture, where only nearest-neighbor interactions are available for two-qubit gates, and an excess amount of quantum swap gates have to be added to the circuit to perform two-qubit gates between qubits distant in space.

We have also carried out a systematic study on several variables that can affect the performance of the fault-tolerant QEC procedure for the three-qubit bit-flip code. Our results show that both collective bath and imperfect projective measurements have minor effects on the threshold value. However, changing the repetition protocol and level of parallelism can significantly change the performance of the fault-tolerant QEC procedure. Our density matrix results indicate that accepting a syndrome only when two consecutive syndrome detections agree (protocol B), which reduces the number of required syndrome detection steps, is the optimal repetition protocol. Compared to the simple majority vote algorithm (protocol A), protocol B increases the efficiency of fault-tolerant QEC at least by a factor of 2. Regarding the level of parallelism in the syndrome detection circuit, in general, a higher level of parallelism results in a more efficient fault-tolerant QEC circuit. The improvement cannot be fully explained by the shorter operational time for a more parallelized circuit; we suggest the major contribution for the improvement comes from the reduction of possible pathways for error propagation. Since the level of parallelism is actually limited by available physical resources in reality, it will be interesting to examine and simulate this factor according to a specific physical implementation of quantum computers (such as ion traps or NMR).

Finally, we emphasize that without specifying the specific noise model and physical device conditions, noise threshold values are of little use. Our noise model is based on well-defined parameters that reflect realistic device conditions and provides a full description for the dissipative dynamics of the quantum computer. As a result, this noise model enables us to access the real performance of fault-tolerant QEC for individual physical implementations. We believe that such information can be useful for the design and optimization of quantum computers.

ACKNOWLEDGMENT

This work was supported in part by the MRSEC Program of the National Science Foundation under Award No. DMR 02-13282.

[1] M. Nielsen and I. Chuang, *Quantum Computation and Quantum Information* (Cambridge University Press, Cambridge, England, 2000).
[2] P. W. Shor, in *Proceedings of the 37th Symposium on Foundations of Computing* (IEEE Computer Society Press, Los Alamitos, CA, 1996), p. 56; e-print quant-ph/9605011.
[3] D. P. DiVincenzo and P. W. Shor, Phys. Rev. Lett. **77**, 3260 (1996).
[4] D. Gottesman, Phys. Rev. A **57**, 127 (1998).
[5] C. Zalka, e-print quant-ph/9612028.
[6] D. Aharonov and M. Ben-Or, in *Proceedings of the Twenty-ninth Annual ACM Symposium on Theory of Computing* (ACM Press, New York, 1997), pp. 46; e-print quant-ph/9611025.
[7] E. Knill, R. Laflamme, and W. Zurek, Proc. R. Soc. London, Ser. A **454**, 365 (1998).
[8] J. Preskill, Proc. R. Soc. London, Ser. A **454**, 385 (1998).
[9] D. Gottesman, e-print quant-ph/9705052.
[10] A. Steane, Nature (London) **399**, 124 (1999).
[11] A. M. Steane, Phys. Rev. A **68**, 042322 (2003).
[12] B. W. Reichardt, e-print quant-ph/0406025.
[13] Y. C. Cheng and R. J. Silbey, Phys. Rev. A **69**, 052325 (2004).
[14] D. Gottesman and I. Chuang, Nature (London) **402**, 390 (1999).
[15] H. Haken and G. Strobl, Z. Phys. **262**, 135 (1968).
[16] A. E. Fowler, C. D. Hill, and L. C. L. Hollenberg, Phys. Rev. A **69**, 042314 (2004).
[17] A. R. Calderbank and P. W. Shor, Phys. Rev. A **54**, 1098 (1996).
[18] A. M. Steane, Phys. Rev. Lett. **77**, 793 (1996).
[19] P. W. Shor, Phys. Rev. A **52**, R2493 (1995).
[20] A. M. Steane, e-print quant-ph/0202036.
[21] C. H. Bennett, D. P. DiVincenzo, J. A. Smolin, and W. K. Wootters, Phys. Rev. A **54**, 3824 (1996).
[22] R. Laflamme, C. Miquel, J. P. Paz, and W. H. Zurek, Phys. Rev. Lett. **77**, 198 (1996).
[23] E. Knill, R. Laflamme, R. Martinez, and C. Negrevergne, Phys. Rev. Lett. **86**, 5811 (2001).
[24] J. I. Cirac and P. Zoller, Phys. Rev. Lett. **74**, 4091 (1995).
[25] D. Wineland *et al.*, Philos. Trans. R. Soc. London, Ser. A **361**, 1349 (2003).
[26] A. Steane, Fortschr. Phys. **46**, 443 (1998).
[27] G. Palma, K.-A. Suominen, and A. Ekert, Proc. R. Soc. London, Ser. A **452**, 567 (1996).
[28] D. A. Lidar, I. L. Chuang, and K. B. Whaley, Phys. Rev. Lett. **81**, 2594 (1998).
[29] D. Bacon, D. A. Lidar, and K. B. Whaley, Phys. Rev. A **60**, 1944 (1999).
[30] P. Kwiat, A. Berglund, J. Altepeter, and A. White, Science

290, 498 (2000).
[31] L. Viola, E. Fortunato, M. Pravia, E. Knill, R. Laflamme, and D. Cory, Science **293**, 2059 (2001).
[32] M. Bourennane, M. Eibl, S. Gaertner, C. Kurtsiefer, A. Cabello, and H. Weinfurter, Phys. Rev. Lett. **92**, 107901 (2004).
[33] J. B. Altepeter, P. G. Hadley, S. M. Wendelken, A. J. Berglund, and P. G. Kwiat, Phys. Rev. Lett. **92**, 147901 (2004).
[34] D. Bacon, J. Kempe, D. A. Lidar, and K. B. Whaley, Phys. Rev. Lett. **85**, 1758 (2000).
[35] D. DiVincenzo, D. Bacon, J. Kempe, G. Burkard, and K. Whaley, Nature (London) **408**, 339 (2000).
[36] J. Kempe, D. Bacon, D. Lidar, and K. Whaley, Phys. Rev. A **63**, 042307 (2001).
[37] D. A. Lidar, D. Bacon, and K. B. Whaley, Phys. Rev. Lett. **82**, 4556 (1999).
[38] D. Bacon, K. Brown, and K. Whaley, Phys. Rev. Lett. **87**, 247902 (2001).
[39] M. B. Plenio, V. Vedral, and P. L. Knight, Phys. Rev. A **55**, 4593 (1997).
[40] B. Kane, Nature (London) **393**, 133 (1998).